Available online at www.sciencedirect.com
SCIENCE DIRECT®
Journal of Chromatography A, 1008 (2003) 23–41
JOURNAL OF CHROMATOGRAPHY A
www.elsevier.com/locate/chroma

Band splitting in overloaded isocratic elution chromatography II. New competitive adsorption isotherms

Fabrice Gritti[a,b], Georges Guiochon[a,b,*]

[a]*Department of Chemistry, University of Tennessee, Knoxville, TN 37996-1600, USA*
[b]*Division of Chemical Sciences, Oak Ridge National Laboratory, Oak Ridge, TN 37831-6120, USA*

Received 27 February 2003; received in revised form 26 May 2003; accepted 26 May 2003

Abstract

The equations of two new binary competitive isotherms models are derived. The first of these models assumes that the isotherms of the two pure, single compounds have distinct monolayer capacities. Its derivation is based on kinetic arguments. The ideal adsorbed solution (IAS) framework was applied to derive the second model that is a thermodynamically consistent competitive isotherm. This second model predicts the competitive adsorption isotherm behavior of a mixture of two compounds that have single-component adsorption behavior following a BET and/or a Langmuir isotherms. Both models apply well to the binary adsorption of ethylbenzoate and 4-*tert*.-butylphenol on a Kromasil-C_{18} column (with methanol–water, 62:38, v/v, as the mobile phase). The best single-solute adsorption isotherms of these two compounds are the liquid–solid extended multilayer BET and the Langmuir isotherms, respectively. The kinetic and thermodynamic new competitive models were compared, regarding the accuracy of their prediction of the elution band profiles of mixtures of these two compounds. A better agreement between experimental and calculated profiles was observed with the kinetic model. The IAS model failed because the behavior of the ethylbenzoate/4-*tert*.-butylphenol adsorbed phase mixture is probably non-ideal. The most striking result is the qualitative prediction by these models of the peak splitting of 4-*tert*.-butylphenol during its elution in presence of ethylbenzoate.

Keywords: Band splitting; Adsorption equilibrium; Frontal analysis; Adsorption energy distribution; Ideal adsorbed solution theory; Adsorption isotherms; Mathematical modeling; Toluene; Ethylbenzene

1. Introduction

The profiles of elution bands are largely controlled by the thermodynamics of the phase equilibrium considered, particularly at high concentrations and when the mass transfer kinetics is not very slow [1–3]. Accordingly, the recovery yield and the production rate of a given separation that an industrial unit can achieve depend to a large extent on this thermodynamics, i.e., on the competitive equilibrium isotherms of the feed components. For obvious economic reasons, preparative chromatography must be carried out at high concentrations. Not infrequently, the concentration of the injected sample is even close to that of the saturated solution. Under such conditions, the equilibrium isotherms of the feed components between the two phases of the chro-

*Corresponding author. Department of Chemistry, University of Tennessee, 552 Buehler Hall, Knoxville, TN 37996-1600, USA. Tel.: +1-865-974-0733; fax: +1-865-974-2667.
E-mail address: guiochon@utk.edu (G. Guiochon).

0021-9673/03/$ – see front matter
doi:10.1016/S0021-9673(03)00970-1

matographic system are rarely linear. The stronger the nonlinear behavior of the isotherm at the band maximum concentration, the more skewed the band profile and the lower the resolution of the band from its neighbors, hence the lower the recovery yield and the production rate [1]. Accordingly, this behavior affects also the resolution between bands, even at high column efficiencies [1]. Strong nonlinear behavior is also associated with intense competition for adsorption between components that are not resolved. This competition affects also the band resolution. To a lesser degree, the mass transfer kinetics affects the precise shape of the elution bands, dispersing the profiles predicted by thermodynamics alone and smoothing its edges. For these reasons, the use of computer-assisted optimization in the development of any new application of preparative liquid chromatography requires the prior determination of accurate thermodynamic and kinetic data and the proper modeling of these data, i.e., the derivation of the competitive isotherms of the feed components and of the rate coefficients of the various steps involved in the mass transfer kinetics across the column [1–4].

Numerous methods are available for the acquisition of equilibrium isotherm data and for the derivation of single-component isotherms [1,5]. Frontal analysis (FA) [1,5–7], elution by characteristic point (ECP) [1,8,9], and pulse methods [1,10] are the fastest and the most convenient of them. They have their own advantages and drawbacks which must be taken into account in any specific case, in order to minimize the errors of measurement and the costs [1]. By contrast, investigations of binary or competitive equilibria remain far more limited [11–17]. Because the acquisition of competitive isotherm data by FA or pulse methods is a far more ambitious project than that of the single-component isotherms, the preferred method of derivation of competitive isotherms is from the single-component isotherms of the components of the mixture involved [1,5,11,14,17]. For this purpose, an assumption must be made as to whether the adsorbed and the bulk phases are ideal or not.

In this work, we first derived a new set of competitive adsorption isotherms, on the basis of kinetic arguments, assuming that one of two components may adsorb on the second one but that the converse is forbidden. This first competitive model leads to two possible single-component isotherms, i.e., the isotherms obtained for one component when the concentration of the other one is zero. The extended liquid–solid Brunauer–Emmett–Teller (BET) and the Langmuir isotherms are these two single-component isotherms. From these single-component isotherms, we derived the corresponding thermodynamically consistent competitive isotherm model using the IAS theory. The thermodynamic consistency of this second set of competitive isotherms is guaranteed by the IAS framework. Finally, these two sets of competitive isotherm models are compared with particular attention being paid to the accuracy of their predictions of the experimental band profiles of binary mixtures of ethylbenzoate and 4-*tert*.-butylphenol, using a packed Kromasil-C_{18} column and a mixture of methanol and water as the stationary and mobile phase, respectively. The band profiles of the components of this binary mixture were previously described [18]. They are most unusual, exhibiting an intense splitting of the band of 4-*tert*.-butylphenol. The ability of the new competitive isotherm models to describe this peak splitting effect is discussed.

2. Theory

2.1. Determination of single-component isotherms by frontal analysis

Among the various chromatographic methods available to determine single-component isotherms, FA is the most accurate [1–4]. It consists in the step-wise replacement of a stream of mobile phase percolating through the column with streams of solutions of the studied compound of increasing concentrations, and in the recording of the breakthrough curves at the column outlet. Mass conservation of the solute between the times when the new solution enters the column and when the plateau concentration is reached allows the calculation of the adsorbed amount, q^*, of solute in the stationary phase at equilibrium with a given mobile phase concentration, C [1,5,14]. This amount is best measured by integrating the breakthrough curve (equal

area method) [19]. The adsorbed amount q^* is given by:

$$q^* = \frac{C(V_{eq} - V_0)}{V_a} \quad (1)$$

where V_{eq} and V_0 are the elution volumes of the equivalent area [19] and of the hold-up volume, respectively, and V_a is the volume of stationary phase in the column.

2.2. Models of single-component isotherm

There are many models of single-component isotherms but only two are useful in this work.

2.2.1. The Langmuir isotherm

This model is the most frequently used in studies of liquid–solid chromatographic equilibria, in spite of its semi-empirical nature [5]. It is written:

$$q^* = q_s \cdot \frac{bC}{1 + bC} \quad (2)$$

In this model, q_s is the monolayer saturation capacity of the adsorbent and b is the equilibrium constant of adsorption. This model assumes that the surface of the adsorbent is homogeneous, that the adsorption is localized, and that there are no adsorbate adsorbate interactions.

2.2.2. The extended liquid–solid BET model

The initial model BET model is the one derived by Brunauer, Emmett, and Teller. It is the most widely applied isotherm model in studies of gas–solid equilibria. It assumes multilayer adsorption [5]. It was developed to describe adsorption phenomena in which successive molecular layers of adsorbate form at pressures well below the pressure required for the completion of the monolayer. The formulation of the extension of this model to liquid–solid chromatography was derived and detailed earlier [20]. Its final equation is:

$$q^* = q_s \cdot \frac{b_S C}{(1 - b_L C)(1 - b_L C + b_S C)} \quad (3)$$

where q_s is the monolayer saturation capacity of the adsorbent, b_S is the equilibrium constant for surface adsorption–desorption over the free surface of the adsorbent and b_L is the equilibrium constant for surface adsorption–desorption over a layer of adsorbate molecules. This model accounts for local adsorption.

2.3. Kinetic derivation of a binary competitive adsorption isotherm

2.3.1. Assumptions of the kinetic model

Let A and B stand for the two compounds. The following five assumptions are made in order to complete the isotherm derivation:

(I) The adsorption and the desorption of A and B follow a first order kinetics.
(II) Molecules of both A and B may adsorb on either the solid surface or on adsorbed molecules of A.
(III) Molecules of neither A nor B may adsorb on adsorbed molecules of B.
(IV) The adsorbed phase is composed of a finite number, N, of layers, as shown in Fig. 1.
(V) The total monolayer capacity for A and B are not necessarily the same ($q_{S,A} \neq q_{S,B}$). Both are independent of the number of the layer in the multilayer system.

2.3.2. Definitions

The following parameters are used in the derivation of the adsorption isotherm model:

- $q_{s,A}$ and $q_{s,B}$ are the monolayer capacities of components A and B, respectively.
- θ_0 is the fraction of the surface area of the adsorbent that is free from adsorbate.
- $\theta_{A,i}$ is the fraction of the surface area of layer i

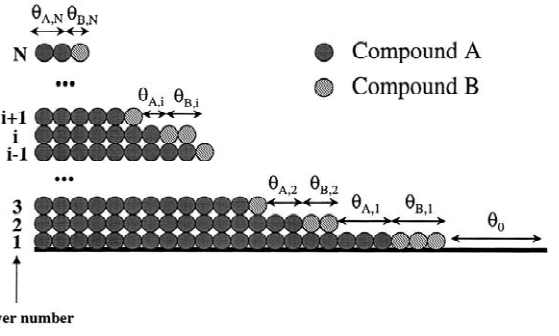

Fig. 1. Scheme of the two-component adsorption model. Note the resulting structure of the adsorbed system due to the non-adsorption on compound B.

that is occupied by molecules of A, and that is not covered by any higher layer of adsorbate molecules (with $1 < i < N$).
- $\theta_{B,i}$ is the fraction of the surface area of layer i that is occupied by molecules of B, and, according to the assumptions of the model, cannot be covered by any other molecules (with $1 < i < N$).
- C_A and C_B are the concentration of compounds A and B in the mobile phase, respectively.
- q_A and q_B are the concentration of compounds A and B in the adsorbed phase, respectively.
- $k^a_{S,A}$ and $k^d_{S,A}$ are the rate constants of adsorption and desorption of compound A on the solid surface, respectively.
- $k^a_{S,B}$ and $k^d_{S,B}$ are the rate constants of adsorption and desorption of compound B on the solid surface, respectively.
- $k^a_{L,A}$ and $k^d_{L,A}$ are the rate constants of adsorption and desorption of compound A on any intermediate local layer of compound A made on the solid surface, respectively.
- $k^a_{L,B}$ and $k^d_{L,B}$ are the rate constants of adsorption and desorption of compound B on any intermediate local layer of compound A made on the solid surface, respectively.

2.3.3. Combinations of parameters
- The ratios $b_{S,A} = k^a_{S,A}/k^d_{S,A}$ and $b_{L,A} = k^a_{L,A}/k^d_{L,A}$ are the equilibrium constants of adsorption of compound A onto the free solid surface and onto a layer made of molecules of A, respectively.
- The ratios $b_{S,B} = k^a_{S,B}/k^d_{S,B}$ and $b_{L,B} = k^a_{L,B}/k^d_{L,B}$ are the equilibrium constants of adsorption of compound B onto the free solid surface and onto a layer made of molecules of A, respectively.
- $r_{X,A} = k^d_{L,X}/k^d_{S,A}$, with X = A or B.
- $t_{B,A} = k^d_{L,B}/k^d_{L,A}$.

2.3.4. Derivation of the amounts adsorbed

From these assumptions and definitions, one can calculate the amounts of compounds A and B that are adsorbed at equilibrium on the stationary phase. If we keep in mind that the molecules of compound B are never covered by molecules of another compound (either A or B), it is easily demonstrated that (see Fig. 1):

$$q_A = q_{s,A} \sum_{i=1}^{i=N} \left[i\theta_{A,i} + (i-1)\theta_{B,i} \right] \quad (4)$$

$$q_B = q_{s,B} \sum_{i=1}^{i=N} \theta_{B,i} \quad (5)$$

The principle of the kinetic method used now to derive the competitive equilibrium isotherms of A and B consists in writing the $2N + 1$ surface fractions occupied by the free surface and by components A and B in each of the $1 < i < N$ layers making the adsorbed phase. Then, we write equilibrium as:

$$\frac{\partial \theta_{A,i}}{\partial t} = 0 \qquad \frac{\partial \theta_{B,i}}{\partial t} = 0 \quad \text{with} \quad 1 < i < N \quad (6)$$

Since there are N layers, this gives $2N$ equations. The normalization condition of the surface fractions gives the last equation:

$$\theta_0 + \sum_{i=1}^{i=N} \left[\theta_{A,i} + \theta_{B,i} \right] = 1 \quad (7)$$

We now derive the system of equations for each layer. In the rest of this section, we use a separate reference system for the equations. The equations are labeled with a double rank corresponding, the first to the rank of the equation systems that will be derived, the second to the rank of the layer considered, and with a letter A or B depending on the corresponding compound for which the equation is written. Thus, the equation labelled (2-iB) is the equation of the second system stating equilibrium in layer i for compound B.

2.3.4.1. Development of the system of equations

Adsorption–desorption equilibrium on the first layer. There are three ways for the surface fraction $\theta_{A,1}$ to increase:
- When A adsorbs on the free surface θ_0.
- When A desorbs from the second layer.
- When B desorbs from the second layer.

By contrast, there are three ways that the surface fraction $\theta_{A,1}$ may decrease:
- When A adsorbs on the first layer.
- When B adsorbs on the first layer.
- When A desorbs from the first layer.

These different processes may be written as follows:

$$k^{a}_{S,A}C_A\theta_0 + k^{d}_{L,A}\theta_{A,2} + k^{d}_{L,B}\theta_{B,2} - k^{a}_{L,A}C_A\theta_{A,1} - k^{a}_{L,B}C_B\theta_{A,1} - k^{d}_{S,A}\theta_{A,1} = 0 \quad (1\text{-}1A)$$

For compound B, the situation is simpler. The surface fraction $\theta_{B,1}$ increases when B adsorbs on the free surface area, θ_0, and it decreases when B desorbs from the first layer. According to our assumptions, all other events do not affect $\theta_{B,1}$. Hence:

$$k^{a}_{S,B}C_B\,\theta_0 - k^{d}_{S,B}\theta_{B,1} = 0 \quad (1\text{-}1B)$$

Adsorption–desorption equilibrium on the second layer. By iteration to the second layer, we obtain a similar pair of equations for the variation of the surface fractions $\theta_{A,2}$ and $\theta_{B,2}$:

$$k^{a}_{L,A}C_A\theta_{A,1} + k^{d}_{L,A}\theta_{A,3} + k^{d}_{L,B}\theta_{B,3} - k^{a}_{L,A}C_A\theta_{A,2} - k^{a}_{L,B}C_B\theta_{A,2} - k^{d}_{L,A}\theta_{A,2} = 0 \quad (1\text{-}2A)$$

$$k^{a}_{L,B}C_B\theta_{A,1} - k^{d}_{L,B}\theta_{B,2} = 0 \quad (1\text{-}2B)$$

This result is easily generalized to the cases of layers i and N.

Adsorption–desorption equilibrium on layer i

The following equations are obtained:

$$k^{a}_{L,A}C_A\theta_{A,i-1} + k^{d}_{L,A}\theta_{A,i+1} + k^{d}_{L,B}\theta_{B,i+1} - k^{a}_{L,A}C_A\theta_{A,i} - k^{a}_{L,B}C_B\theta_{A,i} - k^{d}_{L,A}\theta_{A,i} = 0 \quad (1\text{-}iA)$$

$$k^{a}_{L,B}C_B\theta_{A,i-1} - k^{d}_{L,B}\theta_{B,i} = 0 \quad (1\text{-}iB)$$

Adsorption–desorption equilibrium on layer N

The following equations are obtained:

$$k^{a}_{L,A}C_A\theta_{A,N\text{-}1} - k^{d}_{L,A}\theta_{A,N} = 0 \quad (1\text{-}NA)$$

$$k^{a}_{L,B}C_B\theta_{A,N-1} - k^{d}_{L,B}\,\theta_{B,N} = 0 \quad (1\text{-}NB)$$

2.3.4.2. Resolution of the system of equation

Using the definitions and notations defined earlier, the system of $2N + 1$ equations just derived can be rewritten as follows:

$$b_{S,A}C_A\theta_0 + r_{A,A}\theta_{A,2} + r_{B,A}\theta_{B,2} - b_{L,A}r_{A,A}C_A\theta_{A,1} - b_{L,B}r_{B,A}C_B\theta_{A,1} - \theta_{A,1} = 0 \quad (2\text{-}1A)$$

$$b_{S,B}C_B\theta_0 - \theta_{B,1} = 0 \quad (2\text{-}1B)$$

$$b_{L,A}C_A\theta_{A,1} + \theta_{A,3} + t_{B,A}\theta_{B,3} - b_{L,A}C_A\theta_{A,2} - b_{L,B}t_{B,A}C_B\theta_{A,2} - \theta_{A,2} = 0 \quad (2\text{-}2A)$$

$$b_{L,B}C_B\theta_{A,1} - \theta_{B,2} = 0 \quad (2\text{-}2B)$$

.....

$$b_{L,A}C_A\theta_{A,i-1} + \theta_{A,i+1} + t_{B,A}\theta_{B,i+1} - b_{L,A}C_A\theta_{A,i} - b_{L,B}t_{B,A}C_B\theta_{A,i} - \theta_{A,i} = 0 \quad (2\text{-}iA)$$

$$b_{L,B}C_B\theta_{A,i-1} - \theta_{B,i} = 0 \quad (2\text{-}iB)$$

.....

$$b_{L,A}C_A\theta_{A,N-1} - \theta_{A,N} = 0 \quad (2\text{-}NA)$$

$$b_{L,B}C_B\theta_{A,N-1} - \theta_{B,N} = 0 \quad (2\text{-}NB)$$

This system of equations must be completed with the normalization condition (Eq. (7)).

We may express the different surface fractions of compound A as linear combinations of surface fractions of A only, eliminating the surface fractions of compound B. Substitution of Eq. (2-2B) into Eq. (2-1A) gives:

$$(1 + b_{L,A}r_{A,A}C_A)\theta_{A,1} = b_{S,A}C_A\theta_0 + r_{A,A}\theta_{A,2} \quad (3\text{-}1A)$$

Following the same procedure for the similar relationships for the third and second layers, we obtain:

$$(1 + b_{L,A}C_A)\theta_{A,2} = b_{L,A}C_A\theta_{A,1} + \theta_{A,3} \quad (3\text{-}2A)$$

For the intermediate equation (layer i), we obtain:

$$(1 + b_{L,A}C_A)\theta_{A,i} = b_{L,A}C_A\theta_{i-1} + \theta_{A,i+1} \quad (3\text{-}iA)$$

And finally, for layer N:

$$\theta_{A,N} = b_{L,A}C_A\theta_{A,N-1} \quad (3\text{-}NA)$$

Eqs. (2-1B)–(2-NB) contain only $\theta_{B,j}$ and, together with Eq. (7), complete the new system of equations.

The next series of equations in the derivation of the isotherm begins with Eq. (3-NA). Then, combining Eqs. (3-NA) and (3-(N−1)A), and continuing with Eqs. (3-(i+1)A) and (3-iA) until Eqs. (3-2A) and (3-1A), gives a series of simpler equations that define an obvious series of equations:

$$\theta_{A,N} = b_{L,A} C_A \theta_{A,N-1} \quad \text{(4-NA)}$$

$$\theta_{A,N-1} = b_{L,A} C_A \theta_{A,N-2} \quad \text{(4-(N-1)A)}$$

.....

$$\theta_{A,i} = b_{L,A} C_A \theta_{A,i-1} \quad \text{(4-iA)}$$

.....

$$\theta_{A,1} = b_{S,A} C_A \theta_0 \quad \text{(4-1A)}$$

Note that the parameters $r_{X,A}$ and $t_{B,A}$ have disappeared. The geometric series is clear. It allows the general solution of the system as:

$$\theta_{A,i} = (b_{L,A} C_A)^{i-1} b_{S,A} C_A \theta_0 \quad \text{(5-iA)}$$

The fractional surface coverages by compound B are now derived from Eqs. (2-1B)–(2-NB), rewritten as:

$$\theta_{B,1} = b_{S,B} C_B \theta_0 \quad \text{(4-B)}$$

.....

$$\theta_{B,i} = b_{L,B} C_B \theta_{A,i-1} \quad \text{(4-iB)}$$

.....

$$\theta_{B,N} = b_{L,B} C_B \theta_{A,N-1} \quad \text{(4-NB)}$$

Hence, the general solution for $i \neq 1$:

$$\theta_{B,i} = b_{L,B} C_B (b_{L,A} C_A)^{i-2} b_{S,A} C_A \theta_0 \quad \text{(5-iB)}$$

The last fractional surface coverage is derived from the normalization condition (Eq. (7)). It is:

$$\theta_0 = \frac{1}{1 + b_{S,B} C_B + b_{S,A} C_A \sum_{i=1}^{i=N} (b_{L,A} C_A)^{i-1} + b_{S,A} C_A b_{L,B} C_B \sum_{i=2}^{i=N} (b_{L,A} C_A)^{i-2}} \quad (8)$$

We can now derive the amounts of A and B adsorbed at equilibrium. For the sake of simplicity in the equations, let:

$$x_A = b_{L,A} C_A \quad y_A = b_{S,A} C_A$$
$$x_B = b_{L,B} C_B \quad y_B = b_{S,B} C_B$$

Eqs. (4) and (5) combined with the equations just derived lead to:

$$\frac{q_A}{q_{s,A}} = \frac{y_A \left(\sum_{i=1}^{i=N} i x_A^{i-1} + x_B \sum_{i=2}^{i=N} (i-1) x_A^{i-2} \right)}{1 + y_B + y_A \sum_{i=1}^{i=N} x_A^{i-1} + y_A x_B \sum_{i=2}^{i=N} x_A^{i-2}} \quad (9)$$

$$\frac{q_B}{q_{s,B}} = \frac{y_B + x_B y_A \sum_{i=2}^{i=N} x_A^{i-2}}{1 + y_B + y_A \sum_{i=1}^{i=N} x_A^{i-1} + y_A x_B \sum_{i=2}^{i=N} x_A^{i-2}} \quad (10)$$

Eqs. (9) and (10) are the exact solutions of the isotherm model if a finite number N of layers is assumed in the competitive model. If an infinite number of layers is assumed in the model, the amounts of A and B adsorbed are easily derived by using the classical limits of the sum of geometric series. So, provided that $x < 1$, we have:

$$\lim_{N\to\infty} \sum_{i=0}^{i=N} x^i = \frac{1}{1-x} \quad \text{and} \quad \lim_{N\to\infty} \sum_{i=1}^{i=N} i x^{i-1} = \frac{1}{(1-x)^2}$$

Accordingly, the limit of the isotherm model for N infinite is:

$$\frac{q_A}{q_{s,A}} = \frac{b_{S,A} C_A + b_{S,A} b_{L,B} C_A C_B}{(1 - b_{L,A} C_A)\left[1 - b_{L,A} C_A + b_{S,A} C_A + b_{S,B} C_B + (b_{S,A} b_{L,B} - b_{S,B} b_{L,A}) C_A C_B\right]} \quad (11)$$

$$\frac{q_B}{q_{s,B}} = \frac{b_{S,B} C_B + (b_{S,A} b_{L,B} - b_{S,B} b_{L,A}) C_A C_B}{1 - b_{L,A} C_A + b_{S,A} C_A + b_{S,B} C_B + (b_{S,A} b_{L,B} - b_{S,B} b_{L,A}) C_A C_B} \quad (12)$$

2.3.4.3. From competitive isotherms to single isotherms

The single component isotherms of A and B can be derived from the competitive isotherms, Eqs. (11) and (12), by letting $C_B = 0$ in Eq. (11) and $C_A = 0$ in Eq. (12). Then, the isotherm equation for A becomes that of the extended liquid–solid BET isotherm [20] (Eq. (3)), which is consistent with the strictures of our multilayer adsorption isotherm model for A. Similarly, the isotherm equation for compound B

becomes that of the Langmuir model, which is also consistent with the model of adsorption isotherm selected for B, which can form only a monolayer.

We note, however, that this model of competitive isotherm is not thermodynamically consistent. In the next section we derive a thermodynamically consistent model of competitive isotherm using the IAS framework.

2.4. Derivation of a thermodynamically consistent binary adsorption isotherm from the single-component isotherms

Under certain conditions, a competitive binary isotherm can be derived from the single-component adsorption isotherms of the two compounds studied. The thermodynamics of solid–liquid equilibrium for ideal, dilute solutions was derived by Radke and Prausnitz [21], following the approach proposed by Myers and Prausnitz [22] for the competitive adsorption of gas mixtures onto solids. This method is applied here to derive the binary adsorption equilibrium isotherm of a mixture in reversed-phase liquid chromatography (RPLC) from the single-component isotherms obtained in the previous section. The framework of this theory is briefly recalled.

2.4.1. Ideal adsorbed solution theory

Assuming thermodynamic equilibrium between the solution–solid interfacial region and the bulk liquid phase, the Gibbs adsorption isotherm relates the spreading pressure, π, applied by the adsorbed phase onto the adsorbent surface S_f, and the excess adsorbed amounts of the components of a three-component system (solute A, solute B, and solvent S) through the following equation:

$$S_f d\pi = n_A^m d\mu_A^a + n_B^m d\mu_B^a \quad (13)$$

where μ_i^a is the chemical potential of component i in the adsorbed phase and n_i^m is the invariant adsorption amount of solute i that can be derived from the variation of the bulk liquid phase that take place upon its contact with the adsorbent [21].

The Gibbs adsorption isotherm derived for liquid–solid adsorption is equivalent to the one for multi-component gas–solid adsorption under the following two conditions [21]: (1) the concentrations of the two mixture components are much lower than that of the solvent (dilute solutions). (2) The adsorption of the solute must be strong.

Eq. (13) becomes:

$$d\pi = \Gamma_A d\mu_A^a + \Gamma_B d\mu_B^a$$
$$\Gamma_i = \frac{n_i^a}{S_f} \qquad \text{(at constant } T\text{)} \quad (14)$$

where Γ_i is the number of mole of solute i adsorbed per unit area of adsorbent. It is related to the number of moles q_i adsorbed at equilibrium in the mixture by a volume V_{ads} by:

$$\Gamma_i = \frac{1}{S_f} q_i V_{ads} \quad (15)$$

In the case of an ideal adsorbed solution, a simple relationship can be derived [21] between the molar fractions z_i of the mixture components adsorbed and the adsorbed amounts of the single components q^*_i, leading to the same spreading pressure as in the mixture:

$$\frac{1}{\Gamma_A + \Gamma_B} = \frac{z_A}{\Gamma^*_A} + \frac{z_B}{\Gamma^*_B} \text{ or}$$
$$\frac{1}{q_A + q_B} = \frac{z_A}{q^*_A} + \frac{z_B}{q^*_B} \quad (16)$$

The thermodynamic condition of equilibrium between the adsorbed and the liquid phases provides an additional relationship between the actual concentrations C_A and C_B in the bulk solution and the molar composition z_i of the adsorbed phase:

$$C_i = C_i^*(\pi) z_i \text{ then}$$
$$1 = \frac{C_A}{C^*_A} + \frac{C_B}{C^*_B} \text{ constant at } T \text{ and } \pi \quad (17)$$

where C^*_A and C^*_B are two functions of C_A and C_B. They are derived from the condition that the single-component spreading pressures are identical to that of the mixture. The integration of the Gibbs adsorption isotherm (Eq. (14) applied for a single compound) gives these relationships:

$$\pi(C^*_i) = \frac{RT}{S_f}\int_0^{C^*_i} \frac{n_i^{a*}(C_i)}{C_i}\,\mathrm{d}C_i = \frac{RTV_{ads}}{S_f}\int_0^{C^*_i} \frac{q^*_i(C_i)}{C_i}\cdot \mathrm{d}C_i \Rightarrow \int_0^{C^*_A} \frac{q^*_A(C_A)}{C_A}\cdot \mathrm{d}C_A = \int_0^{C^*_B} \frac{q^*_B(C_B)}{C_B}\cdot \mathrm{d}C_B \quad (18)$$

The mole fractions, z_i in the ideal adsorbed phase are derived from Eq. (17). Finally, from Eq. (16), the amounts adsorbed q_A and q_B are obtained as functions of C_A and C_B.

As a conclusion, the IAS theory is a simple method for the calculation of adsorption equilibrium concentrations for dilute solutions of strongly adsorbed components, using only data obtained from the single-component adsorption equilibria at the same temperature. This method will now be applied to the case when the single-component isotherms of compounds A and B are the BET and the Langmuir isotherms, respectively.

2.4.2. Derivation of the competitive isotherms from an extended liquid–solid BET and a Langmuir single-component isotherms

The single-component BET isotherm for solute A is:

$$q_A = q_{S,A}\frac{b_{S,A}C_A}{(1-b_{L,A}C_A)(1-b_{L,A}C_A+b_{S,A}C_A)} \quad (19a)$$

The Langmuir single-component isotherm for solute B is:

$$q_B = q_{S,B}\cdot\frac{b_{S,B}C_B}{1+b_{S,B}} \quad (19b)$$

Although these equations are not derived from thermodynamic considerations but from a simple kinetic model assuming multilayer and monolayer adsorption, respectively, we may apply them within the framework of the IAS theory and use them to build up a binary isotherm model. The equations of this binary isotherm model, $q_A(C_A,C_B)$ and $q_B(C_A,C_B)$ will be thermodynamically consistent with regards to the Gibbs isotherm equation (Eq. (14)).

From Eq. (18), with a simple integration, we derive the spreading pressure of the pure component A when the concentration in the bulk mobile phase is C_A:

$$\pi^*_A(C_A) = \frac{RTV_{ads}}{S_f}\int_0^{C_A}\frac{q_{S,A}b_{S,A}}{(1-b_{L,A}C_A)(1-b_{L,A}C_A+b_{S,A}C_A)}\cdot\mathrm{d}C_A = \frac{RTV_{ads}}{S_f}\cdot q_{S,A}\ln\frac{1-b_{L,A}C_A+b_{S,A}C_A}{1-b_{LA}C_A} \quad (20a)$$

For compound B, we obtain:

$$\pi^*_B(C_B) = \frac{RTV_{ads}}{S_f}\int_0^{C_B}\frac{q_{S,B}b_{S,B}}{(1+b_{S,B}C_B)}\cdot\mathrm{d}C_B = \frac{RTV_{ads}}{S_f}q_{S,B}\ln(1+b_{S,B}C_B) \quad (20b)$$

Assume that the adsorbed phase layer is a three dimensional lattice with a fixed number of adsorption sites for each layer. Let q_S be the maximum concentration of adsorption sites available for one monolayer. Then:

$$q_{S,A} = q_{S,B} = q_S$$

Eq. (18) (or the equality between the spreading pressures of the single-components A and B) and Eq. (16) give a simple system of two equations with two unknowns, C^*_A and C^*_B. If the saturation capacities had been different, a more complex system would be derived and only a numerical solution could be given. An analytical solution will be here derived by solving the system:

$$\frac{1-b_{L,A}C^*_A+b_{S,A}C^*_A}{1-b_{L,A}C^*_A}-1-b_{S,B}C^*_B=0 \qquad \frac{C_A}{C^*_A}+\frac{C_B}{C^*_B}=1 \quad (21)$$

This system is equivalent to:

$$C^*_A = \frac{b_{S,A}C_A+b_{S,B}C_B}{b_{S,A}+b_{L,A}b_{S,B}C_B} \qquad C^*_B = \frac{b_{S,A}C_A+b_{S,B}C_B}{b_{S,B}-b_{L,A}b_{S,B}C_A} \quad (22)$$

Finally, from Eq. (17), the concentrations of component 1 and 2 adsorbed at equilibrium with the

bulk liquid phase are:

$$\frac{q_A(C_A,C_B)}{q_S} = \frac{[b_{S,A}+b_{L,A}b_{S,B}C_B]C_A}{(1-b_{L,A}C_A)(1-b_{L,A}C_A+b_{S,A}C_A+b_{S,B}C_B)}$$
$$\frac{q_B(C_A,C_B)}{q_S} = \frac{[b_{S,B}-b_{L,A}b_{S,B}C_A]C_B}{(1-b_{L,A}C_A)(1-b_{L,A}C_A+b_{S,A}C_A+b_{S,B}C_B)} \quad (23)$$

The competitive isotherm must be thermodynamically consistent because the spreading pressure is a state function, since its differential is a total differential. For a dilute ideal solution of two components A and B in a solvent, the Gibbs adsorption isotherm gives this differential. Assume an infinitesimal change in the concentrations C_A and C_B during which the system remains at equilibrium ($\mu_i^a = \mu_i^b$), Then, at constant temperature T, using Eq. (18), the differential $\pi' = \pi/RT$, is also a total differential:

$$d\pi = \Gamma_A d(RT\ln C_A) + \Gamma_B d(RT\ln C_B) \Leftrightarrow d\pi'$$
$$= \frac{\Gamma_A}{C_A}\cdot dC_A + \frac{\Gamma_B}{C_B}\cdot dC_B = \left(\frac{\partial\pi'}{\partial C_A}\right)_{C_B}\cdot dC_A + \left(\frac{\partial\pi'}{\partial C_B}\right)_{C_A}\cdot dC_B \quad (24)$$

The Schwarz theorem states that the mixed second partial derivatives of the function π/RT must be equal to:

$$\frac{\partial}{\partial C_B}\cdot\left(\frac{\partial\pi'}{\partial C_A}\right) = \frac{\partial}{\partial C_A}\cdot\left(\frac{\partial\pi'}{\partial C_B}\right);$$
$$\Gamma_i = \frac{q_i V_{ads}}{S_f} \Leftrightarrow \frac{\partial}{\partial C_B}\cdot\left(\frac{q_A(C_A,C_B)}{C_A}\right) = \frac{\partial}{\partial C_A}\cdot\left(\frac{q_B(C_A,C_B)}{C_B}\right) \quad (25)$$

The calculation of the mixed second partial derivatives of Eq. (25) gives after simplification:

$$\frac{\partial}{\partial C_B}\cdot\left(\frac{\Gamma_A}{C_A}\right) = \frac{\partial}{\partial C_A}\cdot\left(\frac{\Gamma_B}{C_B}\right)$$
$$\frac{\partial}{\partial C_B}\cdot\left(\frac{\Gamma_A}{C_A}\right) = \frac{1}{D^2(C_A,C_B)}$$
$$\cdot b\left(\left[C_{AL,A}^2(b_{S,A}-b_{L,A})b_{L,A}b_{S,B}\right]+C_A\right.$$
$$\left.\cdot\left[2b_{L,A}b_{S,B}(b_{L,A}-b_{S,A})\right]+\left[b_{L,A}b_{S,B}-b_{S,B}b_{S,A}\right]\right)$$
$$D(C_A,C_B) = (1-b_{L,A}C_A)$$
$$\cdot(1-b_{L,A}C_A+b_{S,A}C_A+b_{S,B}C_B) \quad (26)$$

The Schwarz's condition is satisfied which was guaranteed by the framework of the IAS theory.

As a result, Eq. (23) provides a thermodynamically consistent competitive isotherm for a dilute binary mixture in a given solvent, assuming an extended liquid–solid BET and a Langmuir isotherms for the first and second single-components, respectively, and equal saturation capacities.

Eq. (23) is not equivalent to Eqs. (11) and (12), as could have been expected. The assumptions made in the kinetic model are not consistent with the idea of an ideal solution since the interaction of B over A was allowed but the interaction of A over B was forbidden. In the IAS derived model, all the parameters in the competitive isotherm are those from the two single-component isotherms, while in the kinetic model, an additional independent constant is introduced representing the interaction between B over A. Furthermore, in the kinetic model, the saturation capacities can be taken different.

2.5. Modeling of band profiles in high-performance liquid chromatography (HPLC)

The profiles of the overloaded elution bands recorded experimentally were calculated using the equilibrium-dispersive (ED) model of chromatography [1,5,23]. This model assumes instantaneous equilibrium between the mobile and the stationary phases and a finite column efficiency, originating from an apparent axial dispersion coefficient, D_a, that accounts for the dispersive phenomena (molecular and eddy diffusion) and for the non-equilibrium effects that take place in a chromatographic column. The axial dispersion coefficient is:

$$D_a = \frac{uL}{2N} \quad (27)$$

where u is the mobile phase linear velocity, L the column length, and N the number of theoretical plates or apparent efficiency of the column.

In this model, the mass balance equation for a single component is expressed as follows:

$$\frac{\partial C}{\partial t} + u\frac{\partial C}{\partial z} + F\frac{\partial q^*}{\partial t} - D_a\frac{\partial^2 C}{\partial z^2} = 0 \quad (28)$$

where q^* and C are the stationary and the mobile phase concentrations of the adsorbate, respectively, t is the time, z the distance along the column and $F = (1 - \varepsilon)/\varepsilon$ is the phase ratio at the solute concentration, with ε the total column porosity. The concentrations q^* and C are related through the isotherm equation, $q^* = f(C)$.

2.5.1. Initial and boundary conditions for the ED model

At $t = 0$, the concentrations of the solute and the adsorbate in the column are uniformly equal to zero, and the stationary phase is in equilibrium with the pure mobile phase. The boundary conditions used are the classical Dankwerts-type boundary conditions [24] at the inlet and outlet of the column.

2.5.2. Numerical solutions of the ED model

The ED model was solved using the Rouchon program based on the finite difference method [1].

3. Experimental

3.1. Chemicals

The mobile phase used in this work was a mixture of HPLC-grade water–methanol (62:38, v/v), both purchased from Fisher Scientific (Fair Lawn, NJ, USA). The same mobile phase was used for the determination of the single-component adsorption isotherm data and for the recording of large size band profiles of the two single components and of binary mixtures. The solvents used to prepare the mobile phase were filtered before use on an SFCA filter membrane, 0.2 μm pore size (Suwannee, GA, USA).

The solutes used were uracil, 4-*tert*.-butylphenol and ethylbenzoate. All were obtained from Aldrich (Milwaukee, WI, USA).

3.2. Materials

A manufacturer-packed, 250 × 4.6 mm Kromasil column was used (Eka Nobel, Bohus, Sweden, EU). This column was packed with a C_{18}-bonded, end-capped, porous silica. This column (column E6021) was one of the lot of 10 columns previously used by Kele and Guiochon [25] and Gritti and Guiochon [26] (columns E6019, E6103 to E6106, E6021 to E6024 and E6436) for their study of the reproducibility of the chromatographic properties of RPLC columns under linear and non-linear conditions, respectively. The main characteristics of the bare porous silica and of the packing material used are summarized in Table 1.

The hold-up time of this column was derived from the retention time of uracil injections. With a mobile phase composition of 62:38, the elution time of uracil is nearly the same as that of pure methanol or sodium nitrate. The product of this time and the mobile phase flow-rate gives an excellent estimate of the column void volume. The void volume of the column and its total porosity ϵ_T in methanol–water (62:38, v/v) mobile phase are 2.40 ml and 0.5769, respectively.

3.3. Apparatus

The isotherm data were acquired using a Hewlett-Packard (Palo Alto, CA, USA) HP 1090 liquid chromatograph. This instrument includes a multi-solvent delivery system (tank volume, 1 l each), an autosampler with a 25 μl loop, a diode-array UV detector, a column thermostat and a computer data acquisition station. Compressed nitrogen and helium bottles (National Welders, Charlotte, NC, USA) are connected to the instrument to allow the continuous operation of the pump and autosampler and solvent sparging. The extra-column volumes are 0.058 and 0.90 ml as measured from the autosampler and from the pump system, respectively, to the column inlet.

Table 1
Physico-chemical properties of the packed Kromasil-C_{18} (Eka) E6021 column

Particle size	5.98 μm
Particle size distribution (90:10, % ratio)	1.44
Pore size	112 Å
Pore volume	0.88 ml/g
Surface area	314 m^2/g
Na, Al, Fe content	11; <10; <10 ppm
Particle shape	Spherical
Total carbon	20.0%
Surface coverage	3.59 μmol/m^2
Endcapping	Yes

All the retention data were corrected for this contribution. The flow-rate accuracy was controlled by pumping the pure mobile phase at 23 °C and 1 ml/min during 50 min, from each pump head, successively, into a 50-ml volumetric glass. A relative error of less than 0.4% was obtained so that we can estimate the long-term accuracy of the flow-rate at 4 μl/min at flow-rates around 1 ml/min. All measurements were carried out at a constant temperature of 23 °C, fixed by the laboratory air-conditioner. The daily variation of the ambient temperature never exceeded 1 °C.

3.4. Isotherm measurements by frontal analysis

The mobile phase composition at which single-component FA measurements are performed is first chosen depending on the retention factor of the solutes at infinite dilution. In order to be able to acquire a sufficient number of data points and to achieve measurements of a satisfactory accuracy, the retention factor should be neither too high nor too low. Values between 1and 5 are usually ideal. In this study, the mobile phase composition will be also constrained by the nature of the isotherm of the two solutes involved, as we expect them to be for the competitive models. As it will be shown later, for the methanol–water composition of 62:32 selected in this work, the isotherm of ethylbenzoate is well described by the extended BET model. The limit retention factor at infinite dilution is between 4 and 5, which is an ideal situation for FA measurements. Too high a methanol concentration would have given a nearly linear isotherm, with which competitive behavior would not have been easily modeled. The isotherm of 4-*tert*.-butylphenol is well accounted for by a Langmuir isotherm model. Because the retention factor is rather high at of about 7, only 26 data points were acquired instead of at least 30 as usually done. Prior to the isotherm determinations, approximate values of the solubilities of 4-*tert*.-butylphenol and ethylbenzoate in the mobile phase at 23 °C were determined by stepwise additions of 0.5 ml of the pure mobile phase into a volume of 25 ml of a saturated solution, until complete dissolution. Accordingly, the maximum concentrations used in the FA measurements were 50 and 40 g/l for 4-*tert*.-butylphenol and ethylbenzoate, respectively.

One pump of the HPLC instrument was used to deliver a stream of the pure mobile phase, the second pump, a stream of the concentrated sample solution. The concentration of the studied compound in each FA run is determined by the concentration of the mother sample solution and the flow-rate fractions delivered by the two pumps. The breakthrough curves are recorded successively, at a flow-rate of 1 ml^3/min, with a sufficiently long time delay between each breakthrough curve to allow for the reequilibration of the column with the pure mobile phase. The injection time of the sample was kept constant at 6 min for 4-*tert*.-butylphenol in order to reach a stable plateau at the column outlet. For ethylbenzoate, the injection time of the sample depends on the time required to reach the plateau concentration and is progressively increased from 5 to 8 min. To avoid any UV-absorption superior to 1500 mAU and increasing noise for each individual solutes, the signals of 4-*tert*.-butylphenol and ethylbenzoate were both detected with the UV detector at 295 nm. The overloaded profiles needed for the validation of the fitted isotherms were recorded after all the frontal analysis experiments were done.

3.5. Recording of the single-component injections

We recorded three types of profiles. The corresponding injections lasted 0.30 min at 10% of the maximum concentration applied in the FA measurement, 1.00 min at 50%, and 2.00 min at 90% of this concentration. The boundary conditions used for the calculation of the chromatograms of 4-*tert*.-butylphenol and ethylbenzoate were assimilated to rectangular profiles.

3.6. Recording of the two-solute mixture band profile

A mixture of 4-*tert*.-butylphenol and ethylbenzoate (40 g/l each) was injected into the column, using the solvent delivery system. The time of injection (120 s) was chosen long enough to maximize the competition between the two solutes in the column. The corresponding band profile was measured accurately by collecting 43 fractions of 300 μl (i.e., 22 droplets each), at a constant flow-rate of

1 ml/min, between the elution time of 11 min to that of 24 min. Aliquots of 10 μl of the 43 fractions were injected into the column using a methanol–water (70:30, v/v) mixture as the mobile phase. After preliminary calibration, the measurement of the areas of the two separated peaks allowed the determination of the concentration of each individual component in the corresponding collected fraction. The individual and total band profiles in the mixed zone are reconstituted by assigning a time to each fraction. This time is determined by the actual collection time minus the time needed for the mobile phase to percolate through the capillary joining the detector cell and the collector vials (10 s at 1 ml/min).

The boundary condition used for the calculation of the chromatograms of the mixtures of 4-*tert*.-butylphenol and ethylbenzoate was assimilated to a rectangular profile.

4. Results and discussion

4.1. Measurement and validation of the two single isotherms

Fig. 2A shows the experimental adsorption isotherm data acquired by frontal analysis for 4-*tert*.-butylphenol and ethylbenzoate (symbols). These data were measured on the C_{18}-Kromasil column phase using a methanol–water (62:38, v/v) mixture as the mobile phase. These two isotherms have very different shapes. The isotherm of ethylbenzoate is an anti-Langmuirian isotherm while that of 4-*tert*.-butylphenol is langmuirian. Fig. 2B demonstrates that, under linear conditions, 4-*tert*.-butylphenol is more retained than ethylbenzoate at infinite dilution. The initial slope of the former isotherm (i.e., its Henry constant) is higher than that of the later. In the low concentration range, the isotherm of 4-*tert*.-butylphenol is above that of ethylbenzoate. However, a clear reversal of the elution order takes place at some intermediate concentration close to 5.5 g/l.

The isotherm data of 4-*tert*.-butylphenol are well accounted for by a simple Langmuir model (Fisher number = 4022). The continuous line on Fig. 2 represents the best Langmuir isotherm. However, a Toth isotherm [27,28] leads to a still better fit (Fisher number = 38 320), an improvement that is significant

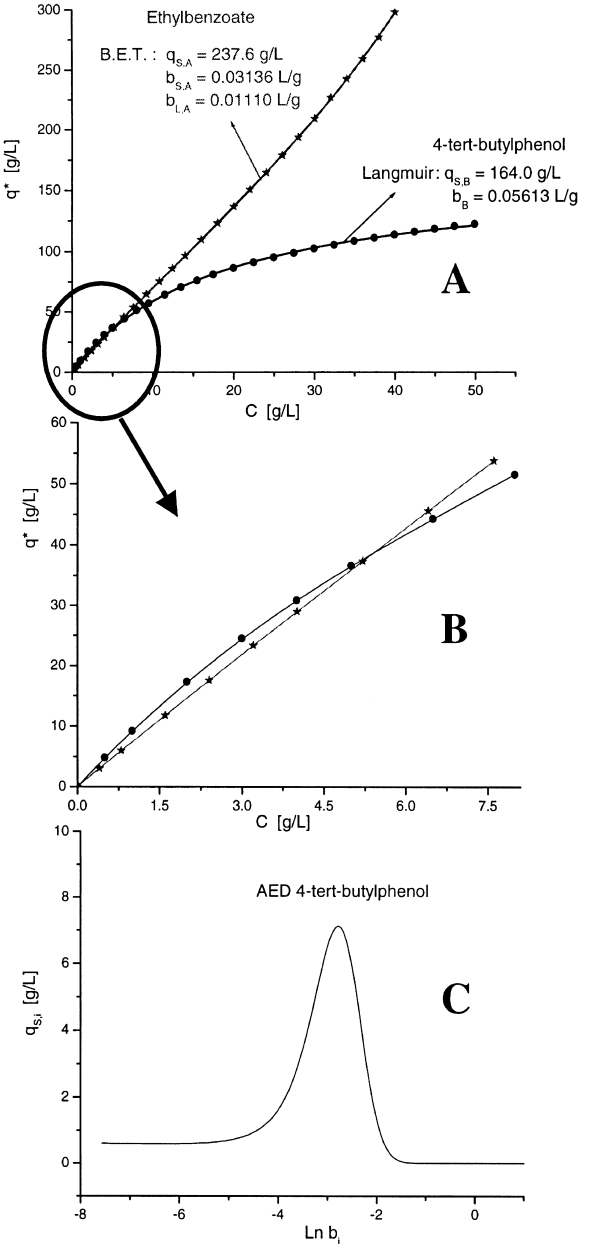

Fig. 2. (A) Experimental single-component isotherm data (symbols) of ethylbenzoate (connected stars) and 4-*tert*.-butylphenol (connected circles) on the packed Kromasil-C_{18} column with methanol–water (62:38, v/v) as the mobile phase. The solid lines are the best fitting isotherms using the extended liquid–solid BET and Langmuir isotherm models. T = 295 K. (B) Zoom of the initial part of the experimental isotherm plots. Note the higher Henry constant for the langmuirian compound. (C) Adsorption energy distribution derived from the FA data of 4-*tert*.-butylphenol. Note the unimodal distribution slightly skewed toward the lower energies.

despite the higher number of parameters in the model (3 instead of 2). The validity of this model is confirmed by the adsorption energy distribution calculated directly from the raw adsorption data (Fig. 2C): the energy distribution is unimodal but unsymmetrical. It tails slightly toward the low energies (as expected for a Toth isotherm) but is clearly not a bimodal distribution (eliminating the Bi-Langmuir isotherm as a model of the isotherm data). In the context of our purpose, the study of the competitive isotherm behavior of the two compounds and the calculation of their band profiles, we will assume a langmuirian adsorption behavior. Note that the values of the two parameters of the Langmuir model ($q_S = 164$ g/l and $b = 0.05613$ l/g) are consistent with those measured on a packed C_{18} Symmetry column eluted with a methanol–water (60:40, v/v) mixture as the mobile phase ($q_S = 141$ g/l and $b = 0.0619$ l/g) [29]. The use of the Langmuir model to calculate the profiles of three large bands gives results in excellent agreement with the experimental profiles (Fig. 3A).

The isotherm of ethylbenzoate is well accounted for by a liquid–solid extended BET isotherm model. The excellent agreement is characterized by a high Fisher number of 46 850. This result was expected since two homologous analytes, butyl- and propylbenzoates, exhibit this same adsorption isotherm behavior in a most similar mobile phase, containing 65% of methanol [29,30]. The effects of a decrease of the length of the alkyl chain compensates that of a decrease of the methanol content of the mobile phase and their balance avoids a ''linearization'' or a ''Langmuirization'' of the isotherm [29]. Attempts to fit the adsorption data to an anti-Langmuir or a quadratic model failed because, giving low Fisher numbers and isotherm parameters that have no physical sense. The best parameters found for q_S, b_S, and b_L were 237.7 g/l, 0.03136 l/g and 0.0111 l/g, respectively. Again, a comparison can be made with the results obtained with butylbenzoate on the Symmetry column eluted with a solution of methanol–water (65:35, v/v) [29]. The lower saturation capacity (164 g/l) may be explained, in part, by the larger size of the molecule of butylbenzoate, which cannot penetrate as deeply as ethylbenzoate amidst the octadecyl chains. As expected, the adsorption constants are larger because butylbenzoate, having two more carbon atoms in the alkyl chain, is more hydrophobic than ethylbenzoate. Both adsorption constants were about three times larger (0.0980 and 0.0396 l/g for b_S and b_L, instead of 0.03136 and 0.0111 l/g, respectively) than those found for ethylbenzoate. Finally, a good agreement is obtained between the experimental and the calculated band

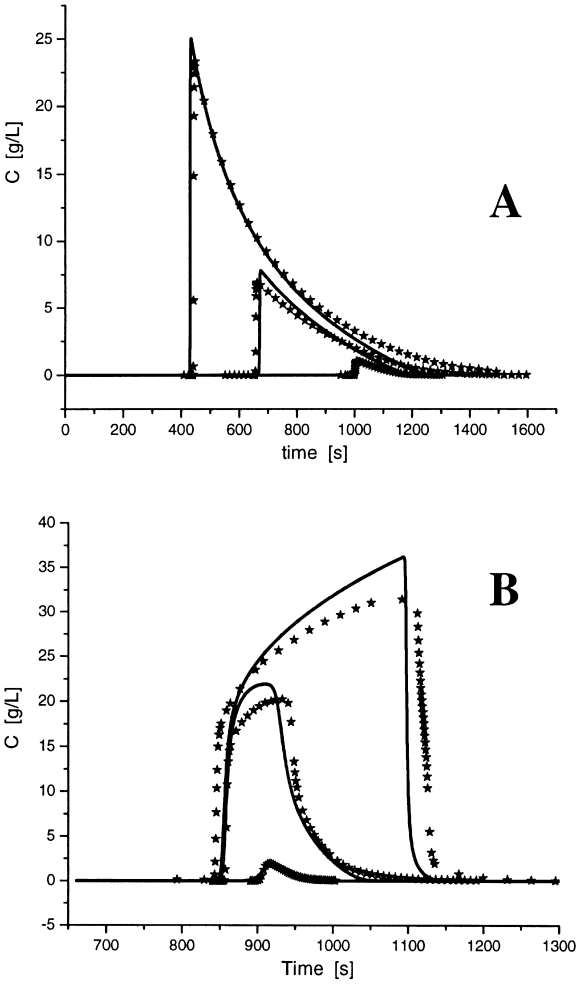

Fig. 3. Comparison between calculated (thick solid line) and experimental (symbols) band profiles of 4-*tert*.-butylphenol and ethylbenzoate on the Kromasil-C_{18} column with methanol–water (62:38, v/v) as the mobile phase. (A) Injection of three solutions of 4-*tert*.-butylphenol at 5.0, 27.5 and 50.0 g/dm^3 during 18 s (L_f 0.5%), 60 s (L_f 9%) and 120 s (L_f 33%), respectively. (B) Injection of a solution of ethylbenzoate at 4.0, 22.0 and 40.0 g/dm^3 during 18 s (L_f 0.3%), 90 s (L_f 8%) and 180 s (L_f 29%). Flow-rate 1 cm^3/min, $T = 295$ K.

profiles (Fig. 3B). However, this agreement is not excellent, as it often is, probably because the ED model assumes a constant efficiency and a constant column porosity. Thus, the model of chromatographic behavior used does not accurately predict the experimental band profiles of ethylbenzoate at the highest concentrations, e.g., beyond 15 g/l. It is also probable that the mass transfer kinetics depends on the local solute concentration, as was already observed for butylbenzoate beyond 5 g/l on a C_{18}-bonded monolithic column [31]. The mass transfer kinetics actually slows down at high concentrations so that the ED model predicts too short retention times and too high concentrations in the upper part of the band (Fig. 3B). This explanation compounds with the consequences of a decrease of the particle porosity when multilayer adsorption takes place, an effect which has also some impact on the isotherm calculation [31]. Fig. 4B shows that, at a concentration of ethylbenzoate of 40 g/l in the mobile phase, the equilibrium solid-phase concentration is 300 g/l. As a first approximation, assuming a density of 1 g/l for the adsorbed analyte (the density of the pure liquid is 1.051), the adsorbed ethylbenzoate occupies 22% of the total void volume, a non-negligible volume fraction.

Thus, the adsorption behavior of the compounds selected in the chromatographic system studied here follows a Langmuir model for the first one, an extended liquid–solid BET model for the second. This makes the binary adsorption behavior of their mixtures most suitable for the application of the model of competitive isotherms developed earlier. The comparison of the band profiles measured and calculated with this model will provide a test of the validity of this model.

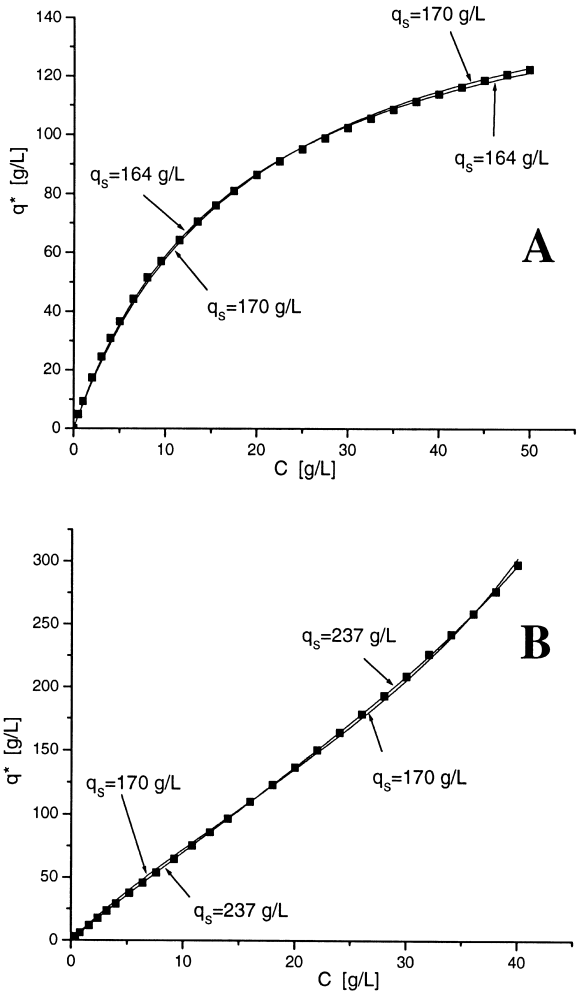

Fig. 4. Comparison between the experimental isotherms (connected squares) of 4-*tert*.-butylphenol (A) and ethylbenzoatene (B) and the best fitting isotherms (solid lines) assuming distinct (q_S for 4-*tert*.-butylphenol = 164 g/l, q_S for ethylbenzoate = 237 g/l) or the same saturation capacities for the two compounds (q_S for 4-*tert*.-butylphenol = q_S for ethylbenzoate = 170 g/l). Note, still, the very good agreement between the experiment and the model.

4.2. Individual band profiles and the IAS competitive model

A sample solution of 4-*tert*.-butylphenol and ethylbenzoate containing 40 g/l of each compound was injected into the column for 120 s. Fractions were collected as explained earlier and analyzed. The individual band profiles of the two components were derived from these analyses (Fig. 5A and B, symbols). The concentration distribution of 4-*tert*.-butylphenol, the compound with a Langmuir isotherm, is split into two parts. The larger mass fraction (ca. 95% in this case) is eluted first, between 8.6 and 17.0 min, as a large band with a front shock and a rear diffuse boundary. Then, the concentration remains very close to zero for about 2 min and, finally, the smaller mass fraction (5%) is eluted as a small langmuirian band, with a front shock and a

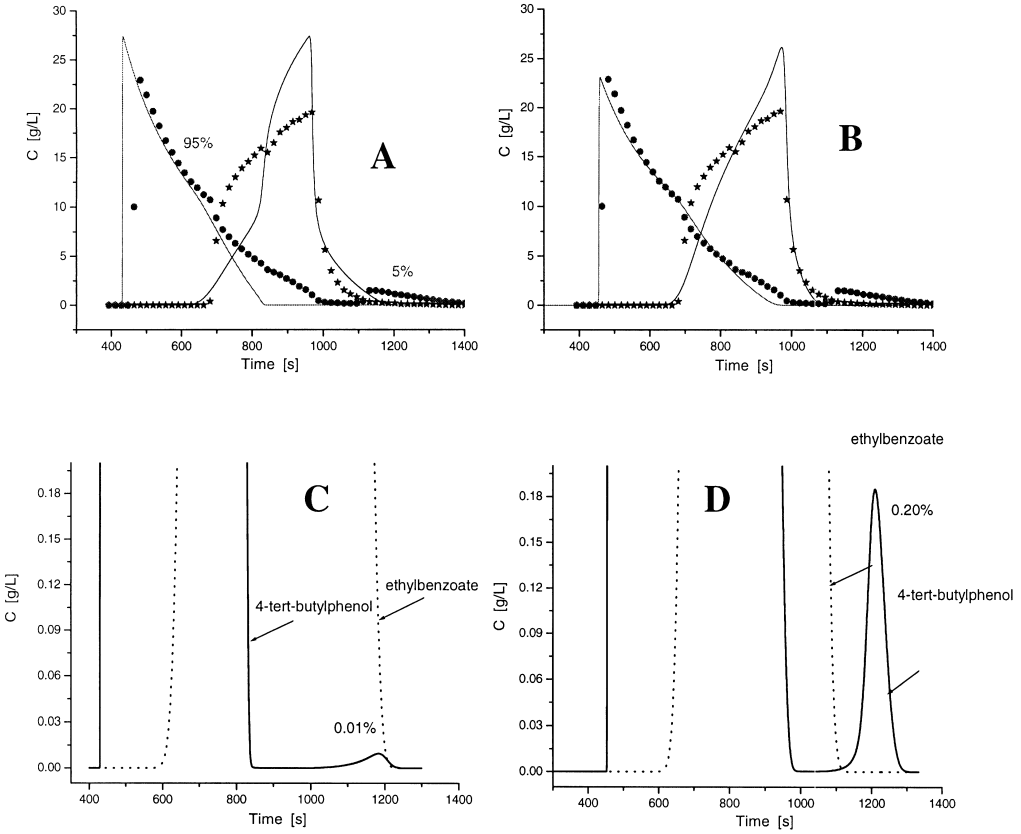

Fig. 5. Upper graphs: Comparison between simulated (solid lines) and experimental individual band profiles (star plots: ethylbenzoate; circle plots: 4-*tert*.-butylphenol). On the left (A), the simulation is using the competitive isotherm model derived by the ideal adsorbed solution (IAS) framework in Eq. (23). On the right (B), the competitive isotherm derived from kinetic argument, whose final result is summarized in Eqs. (11) and (12), is used in the simulation. Note the qualitatively rather better agreement in B. Lower graphs: Zoom at very low outlet concentrations ($C < 0.20$ g/l) of the individual simulated profiles of 4-*tert*.-butylphenol (solid line) and ethylbenzoate (dotted line) using the thermodynamically consistent (C) and the kinetically derived (D) models of competitive isotherms. Note that both models predict the band splitting of 4-*tert*.-butylphenol.

regular rear diffuse boundary. The front of this second band elutes just after completion of the elution of the large band of ethylbenzoate. Such a split band profile is extremely rare and must be related to the unusual reversal of the elution order of the low and the high concentrations. This mirrors the existence of the crossing of the two single-component isotherms as it is observed in Fig. 2.

The validity of the thermodynamically consistent model of competitive isotherms derived earlier (Eq. (23)), using the IAS framework, was first tested. The main advantage of this model is that all its parameters are directly derived from those of the corresponding single-component isotherms. However, to be consistent with the IAS approach, the saturation capacities of both solutes must be the same, yet, they must also give single-component isotherms that are in satisfactory agreement with the experimental isotherm data. Fig. 4 shows that, for both compounds, there is a good agreement between the FA data (symbols) and the best isotherms assuming that the two saturation capacities are equal to 170 g/l. The b value of the Langmuir isotherm becomes 0.05163 g/l, the b_S and b_L constants of the BET

isotherm become 0.05012 and 0.01353 g/l, respectively. The figure illustrates also that the compelling need to modify the parameters of the best single-component isotherms is the major drawback of the use of a thermodynamically consistent model because the saturation capacities of two solutes are actually rarely close.

The results of the band profile calculations carried out within this limitation are shown in Fig. 5A that compares the calculated (solid lines) and the experimental (symbols) individual band profiles. The general aspects of the two band systems are in good global agreement, in spite of some serious local differences. The IAS competitive model fails properly to describe the composition of the mixed elution zone eluted between 650 and 1000 s. Also the front of the band of 4-*tert*.-butylphenol is eluted too early and the model does not seem to account for the band splitting of the phenol. Finally, the profile of the ester band is very different from the one measured by fraction collection. The reversal of the elution order of the two components at high and low concentrations does not seem to have practical consequences in Fig. 5A. Yet, the competitive isotherms predict some degree of band splitting, but a large magnification of the concentrations is needed to visualize the second part of the band (Fig. 5C). Instead of accounting for 5% of the total mass injected, as in the experimental profile, the second part of the calculated band represents only 0.01% of the mass injected.

To better understand the formation of the second peak of the phenol band, we calculated the band profiles obtained for different values of the constant b of the Langmuir isotherm, keeping constant the isotherm parameters of the ester and the injection conditions ($t_p = 120$ s, $C_{1,2} = 40$ g/l, Fig. 6). When b is smaller than b_S (that is when the langmuirian compound is eluted before the BET compound under linear conditions, i.e., Fig. 6A, $b = 0.03$ l/g), no peak splitting is observed. By contrast, for $b = 0.06$ l/g, a value barely larger than $b_S = 0.05012$ l/g, we observe the apparition of a second peak in the band of the langmuirian compound. The mass under this peak is small and represents less than 1% of the total amount injected. When b is increased further, this second peak increases and the two split peaks begin to overlap each other. Among the six cases presented in Fig. 6, however, none can represent correctly the experimental results that we observed. We need a better way to account for the peak splitting.

4.3. Individual band profiles and the kinetic competitive model

Two major differences exist between the IAS model just discussed and the kinetic competitive model initially derived. These are: (1) the two saturation capacities are not supposed to be the same in the kinetic model, so that the parameters of the single component isotherms can be conserved; and (2) one more degree of freedom is available since it is possible to select arbitrarily the value of the constant $b_{L,B}$ of adsorption–desorption of the langmuirian compound (4-*tert*.-butylphenol) over a layer of adsorbed molecules of the anti-langmuirian compound (ethylbenzoate).

The best agreement between the experimental and calculated profiles was obtained for $b_{L,B} = 0.026$ l/g. This value is more than twice the one of ethylbenzoate (0.0111 l/g), which might be explained by the higher hydrophobicity of the *tert*.-butyl group attached to the phenol ring. The isotherms of the two compounds calculated with the IAS theory and with the kinetic model are compared in Fig. 7. The calculated and experimental band profiles are compared in Fig. 5B. The individual profile of ethylbenzoate is far more accurately accounted for with the kinetic model than with the IAS model. The only significant difference between calculated and experimental profiles of the band of ethylbenzoate is at the band top. It mirrors the difference found for the single-component profiles (Fig. 3B). The kinetic model predicts the split of the band profile of *tert*.-butylphenol. However, the significant improvement observed is insufficient. The mass fraction of the second part of the calculated band, at 0.20% of the total amount injected, is still thirty times smaller than the 5% observed experimentally. Numerous attempts at estimating the best model parameters that would predict a second peak having 5% of the injected amount remained unsuccessful. This shows that the kinetic model used here is too simple and must be improved. An obvious improvement could consist in allowing the adsorption of molecules of the anti-langmuirian compound on any layer of molecules of

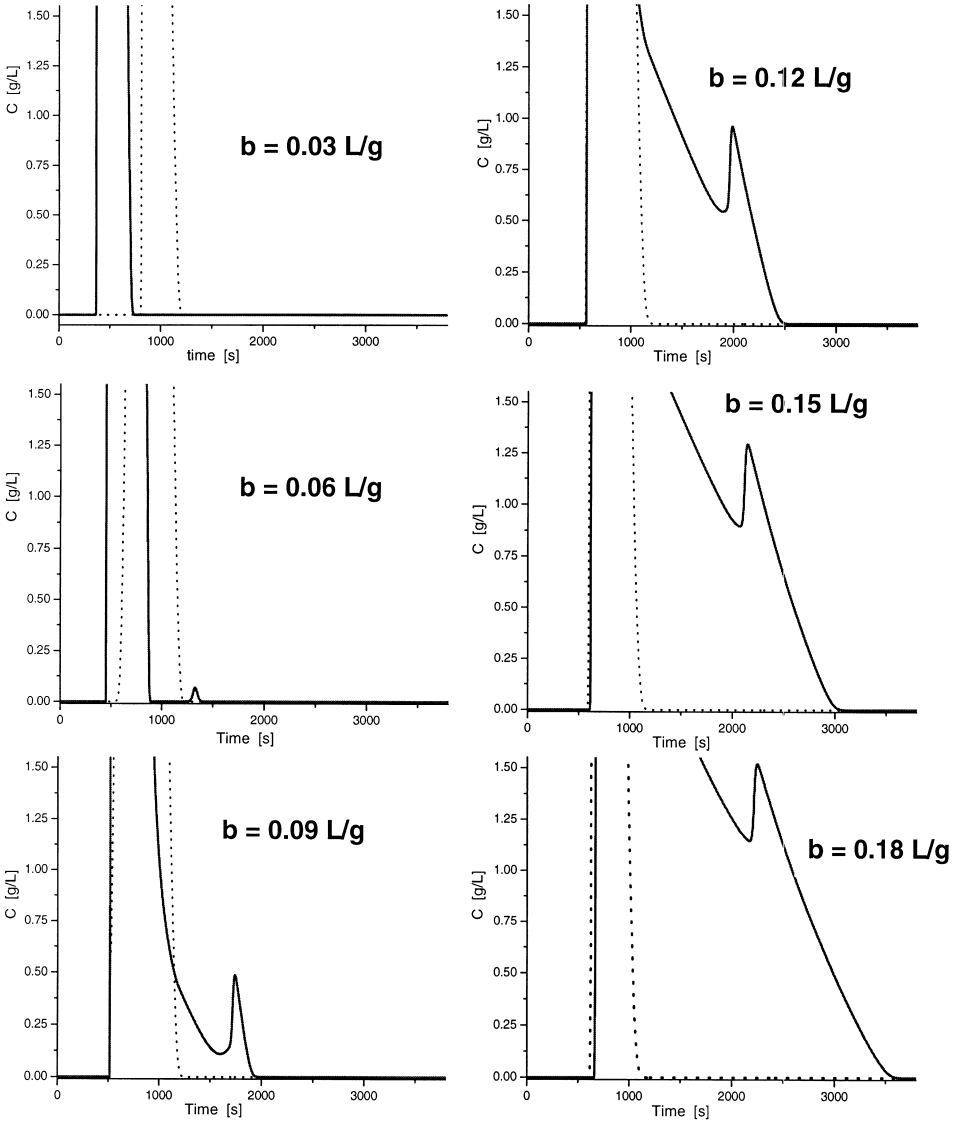

Fig. 6. Influence of the adsorption–desorption constant b of the langmuirian compound (solid line) on the existence of the band splitting during the mixture elution with an anti-langmuirian compound (dotted line). The simulation was carried out with the thermodynamically consistent model described in Eq. (23).

the langmuirian one. The derivation of the corresponding model of binary adsorption is more complex and will be investigated later.

5. Conclusion

Two new competitive isotherm models were derived. The first model uses the ideal adsorbed solution theory to combine the extended liquid–solid BET and the Langmuir single-component isotherms into a binary isotherm model. This competitive model is thermodynamically consistent. The second model was derived from a simple kinetic argument. It is also consistent with the extended liquid–solid BET and the Langmuir isotherms as single-com-

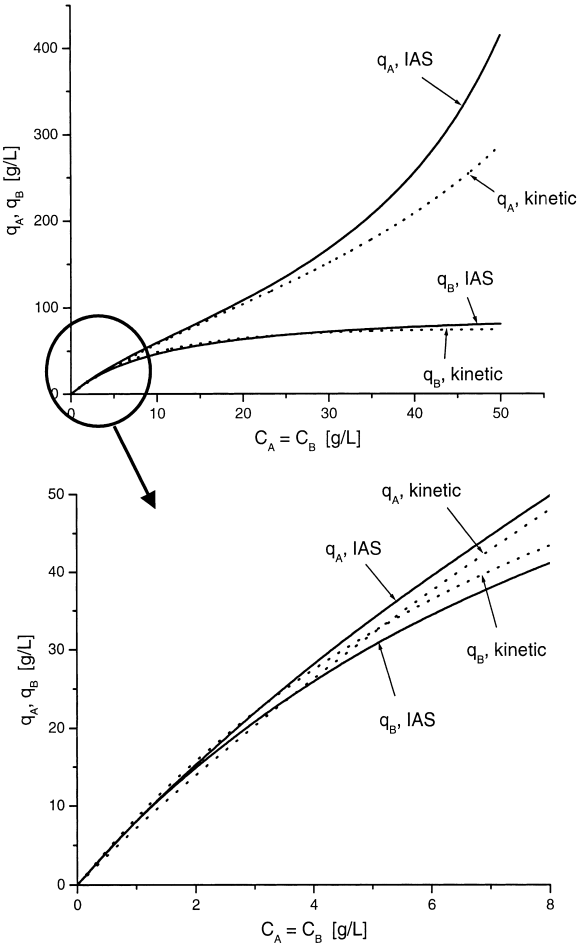

Fig. 7. Comparison of the two calculated competitive isotherms. The IAS model (solid line) and the kinetic model (dotted line) are obtained for the same concentration of the two compounds (see text, Eqs. (11), (12) and (23)).

ponent models for the components of the mixture. These two models were used to calculate the chromatographic band profiles of ethylbenzoate and 4-*tert*.-butylphenol on a C_{18}-bonded silica (Kromasil) column in a solution of methanol–water (62:38, v/v), using the equilibrium-dispersive model of chromatography. The experimental single-component isotherm data of ethylbenzoate and 4-*tert*.-butylphenol are well accounted for by the extended liquid–solid BET and the Langmuir isotherm models, respectively. The calculated and experimental band profiles for the single components are in very good agreement, in spite of some small differences for the profiles of the former compound at high concentrations. The kinetic model predicts globally better than the IAS-derived model the individual band profiles of large amounts of the binary mixture of these two compounds.

Both models predict the peak splitting that is observed for the langmuirian compound and that arises from their different elution order at low and high concentrations. However, the calculated profiles are not accurate. The size calculated for the second peak of the band of 4-*tert*.-butylphenol is only 0.01% with the IAS model, 0.20% with the kinetic model instead of 5% observed experimentally. Work continues to investigate more complex models that could account for the profiles observed. On a more practical viewpoint, the simplicity of the competitive models derived allows fast calculations of band profiles because the time consuming numerical solution of the IAS problem is not necessary.

Acknowledgements

This work was supported in part by grant CHE-00-70548 of the National Science Foundation and by the cooperative agreement between the University of Tennessee and the Oak Ridge National Laboratory. We thank Hans Liliedahl and Lars Torstenson (Eka Nobel, Bohus, Sweden) for the generous gift of the columns used in this work and for fruitful discussions.

References

[1] G. Guiochon, S. Golshan-Shirazi, A.M. Katti, Fundamentals of Preparative and Nonlinear Chromatography, Academic Press, Boston, MA, 1994.
[2] G. Guiochon, J. Chromatogr. A 965 (2002) 129.
[3] B. Lin, G. Guiochon, Modeling for Preparative Chromatography, Elsevier, Amsterdam, 2003.
[4] A. Felinger, G. Guiochon, J. Chromatogr. A 796 (1998) 59.
[5] D.M. Ruthven, Principles of Adsorption and Adsorption Processes, Wiley, New York, 1984.
[6] G. Schay, G. Szekely, Acta Chem. Hung. 5 (1954) 167.
[7] D.H. James, C.S.G. Phillips, J. Chem. Soc. 1954 (1954) 1066.
[8] E. Glueckauf, Trans. Faraday Soc. 51 (1955) 1540.
[9] E. Cremer, G.H. Huber, Angew. Chem. 73 (1961) 461.

[10] F.G. Helfferich, D.L. Peterson, J. Chem. Educ. 41 (1964) 410.
[11] H. Poppe, J. Chromatogr. A 656 (1993) 19.
[12] F. Charton, M. Bailly, G. Guiochon, J. Chromatogr. A 687 (1998) 13.
[13] J.-X. Huang, G. Guiochon, J. Coll. Interf. Sci. 128 (1989) 577.
[14] J. Jacobson, J. Frenz, Cs. Horváth, J. Chromatogr. 316 (1984) 53.
[15] Z. Ma, A. Katti, B. Lin, G. Guiochon, J. Phys. Chem. 94 (1990) 6911.
[16] J. Zhu, A. Katti, G. Guiochon, J. Chromatogr. 552 (1991) 71.
[17] I. Quiñones, J.C. Ford, G. Guiochon, Chem. Eng. Sci. 55 (2000) 909.
[18] F. Gritti, G. Guiochon, J. Chromatogr. A 1008 (2003) 13.
[19] G. Zhong, P. Sajonz, G. Guiochon, Ind. Eng. Chem. (Res.) 36 (1997) 506.
[20] S. Brunauer, P.H. Emmet, E. Teller, J. Am. Chem. Soc. 60 (1938) 309.
[21] C.J. Radke, J.M. Prausnitz, AIChE J. 18 (1972) 761.
[22] A.L. Myers, J.M. Prausnitz, AIChE J. 11 (1965) 121.
[23] M. Suzuki, Adsorption Engineering, Elsevier, Amsterdam, 1990.
[24] P.W. Danckwerts, Chem. Eng. Sci. 2 (1953) 1.
[25] M. Kele, G. Guiochon, J. Chromatogr. A 855 (1999) 423.
[26] F. Gritti, G. Guiochon, J. Chromatogr. A 1003 (2003) 43.
[27] J. Toth, Acta Chem. Hung. 32 (1962) 31.
[28] J. Toth, Acta Chem. Hung. 69 (1971) 311.
[29] F. Gritti, W. Piatkowski, G. Guiochon, J. Chromatogr. A 978 (2002) 81.
[30] W. Piatkowski, D. Antos, F. Gritti, G. Guiochon, J. Chromatogr. 1003 (2003) 73.
[31] F. Gritti, W. Piatkowski, G. Guiochon, J. Chromatogr. A 983 (2003) 51.